P3HT Nanopillars for Organic Photovoltaic Devices Nanoimprinted by AAO Templates

Dian Chen, Wei Zhao, and Thomas P. Russell*

Department of Polymer Science and Engineering, University of Massachusetts, Amherst, Massachusetts 01003, United States

ABSTRACT

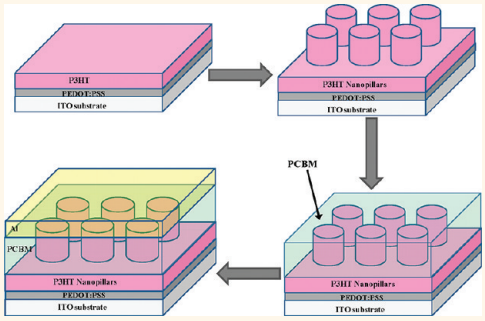

Free-standing nanorod arrays of poly(3-hexylthiophene) (P3HT) were fabricated on indium tin oxide/glass substrates using anodic aluminum oxide (AAO) templates. The AAO templates were treated with a low molecular weight polydimethylsiloxane mold-release agent to reduce their surface energy of the template and interactions with the P3HT. Using a thermal nanoimprinting process, the templates were easily removed, generating nanorods on the surfaces of P3HT thin films. These unique structures were investigated for application in organic photovoltaic devices.

KEYWORDS: nanorod arrays · anodic aluminum oxide · release agent · thermal nanoimprinting · organic photovoltaic devices

During the past decade, organic photovoltaics (OPVs), based on conjugated polymers, have become particularly attractive due to their ease of processing, mechanical flexibility, and low cost for fabricating large-area devices.[1,2] In OPVs, the dissociated free charges (electrons and holes) are generated at the interface between the donor (e-donor) and acceptor (e-acceptor) phases, then transported to their respective electrodes, forming the external circuit. Therefore, increasing the interfacial area between the e-donor and e-acceptor phases and limiting the morphology of the heterojunction to the nanoscale are critical for improving the device performance since the exciton diffusion length in the conjugated polymer is limited to ~10 nm.[3−5] Significant progress has been made in OPV research with the introduction of bulk heterojunction (BHJ) systems. In the BHJ system, the interfacial area between the electron- and hole-transporting domains is increased and, if the domain sizes can be maintained on the tens of nanometer size scale, the increase in the interfacial area is substantial and the domain sizes would be commensurate with the exciton diffusion length. However, the efficiency of converting solar energy into electrical power with plastic solar cells is still not high enough with the most efficient devices having efficiencies of ~8.3% (Konarka Technologies, Inc.). Control over the size scale of the morphology in the active layer, which is normally a kinetically trapped morphology, is achieved by thermal annealing,[6−9] solvent annealing,[10−12] controlling solution concentration and composition,[13,14] adding additives,[15−19] electrospinning,[20] and nanoimprint lithography.[21−25]

Four different OPV device types have been proposed previously. These are (1) single-layer PV cell; (2) bilayer PV cell; (3) disordered bulk heterojunction (the most popular one); and (4) ordered bulk heterojunction.[26] An "ordered bulk heterojunction", consisting of vertically aligned conjugated polymer nanorods surrounded by the e-acceptor materials to form the ordered bicontinuous heterojunction morphology, has been proposed as the ideal morphology for the active layer, yet achieving this morphology has been elusive.[27,28]

Several groups have used nanoimprint lithography (NIL) to produce the polymer nanostructures by using a Si mold.[22,24,25] While making the Si mold with nanometer pore size is expensive, anodic aluminum oxide (AAO) membranes, widely used as templates for fabrication of polymer-based nanostructures, including nanotubes,[29,30] nanorods,[31−34] mesoporous nanostructures,[35,36] and vesicles,[37] provide an inexpensive and effective platform. AAO membranes

* Address correspondence to russell@mail.pse.umass.edu.

Received for review November 9, 2011 and accepted January 5, 2012.

Published online January 05, 2012
10.1021/nn2043548

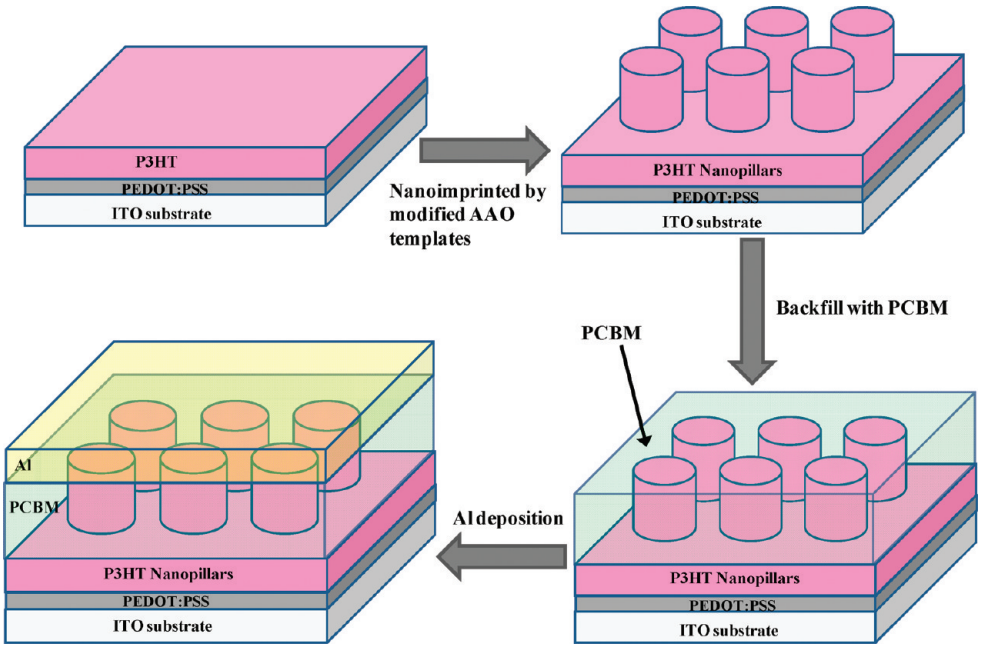

Scheme 1. Procedure for the nanostructured organic photovoltaic device.

characteristically have well-defined pore sizes (ranging from 8 to 500 nm diameter, depending on the anodization conditions) with a narrow pore size distribution, arranged in a hexagonal manner.[38] The surface properties can also be tuned by chemically modifying the surface, taking advantage of hydroxyl groups on the surface of the walls.[39] AAO templates have been used to fabricate poly(3-hexylthiophene) (P3HT) nanopillars,[23,40,41] but the template removal process will dissolve the poly(3,4-ethylenedioxythiophene):poly(styrenesulfonate) (PEDOT:PSS) layer, leaving impurities in the active layer, and in addition, the basic or acidic solution used to remove the template will react with the P3HT, deleteriously affecting the device performance.

To address these problems, we present a simple, cost-effective method to fabricate P3HT nanostructures by using a template method. AAO templates were first modified by PDMS (DMS-T22) to reduce the surface energy of the templates, and the reaction mechanism was explained by Krumpfer and coauthors.[42] After thermal imprinting, the templates were easily removed and free-standing nanorod arrays with controllable domain size were successfully replicated on a P3HT thin film. These free-standing nanorods were then used to fabricate the OPV devices.

RESULTS AND DISCUSSION

The preparation of the nanostructured OPVs based on P3HT nanorod arrays is illustrated in Scheme 1. First, nanostructured P3HT surfaces (e-donor) on the PEDOT:PSS-coated ITO (anode) were prepared by the NIL method. Subsequently, [6,6]-phenyl-C61-butyric acid methyl ester (PCBM) (e-acceptor) was spin-coated directly on top of the P3HT nanostructured layer from a dichloromethane

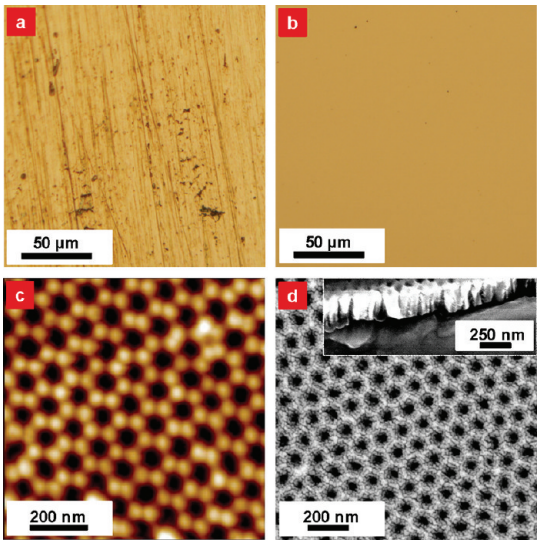

Figure 1. Al sheet and AAO membrane: (a) Al surface before grinding; (b) Al surface after grinding; (c) SFM image of the AAO membrane (second anodization time 1 min); (d) SEM image of the AAO membrane. The inset shows a side view of the AAO membrane.

solution (10 mg/mL). A thin (~100 nm) layer of aluminum (Al) was then thermally evaporated under high vacuum onto the surface (area 6 mm^2) as the cathode.

To be used as an NIL template, the surface of the AAO membrane must be flat and smooth. To achieve this, the original aluminum sheet was polished to a smooth finish. Here, a mechanical polishing method was used instead of the electropolishing method. The surfaces of the aluminum sheet before and after polishing are shown in the Figure 1a,b, respectively. The mirror-like surface shown in Figure 1b is critical for preparing a flat AAO template. After polishing, the AAO

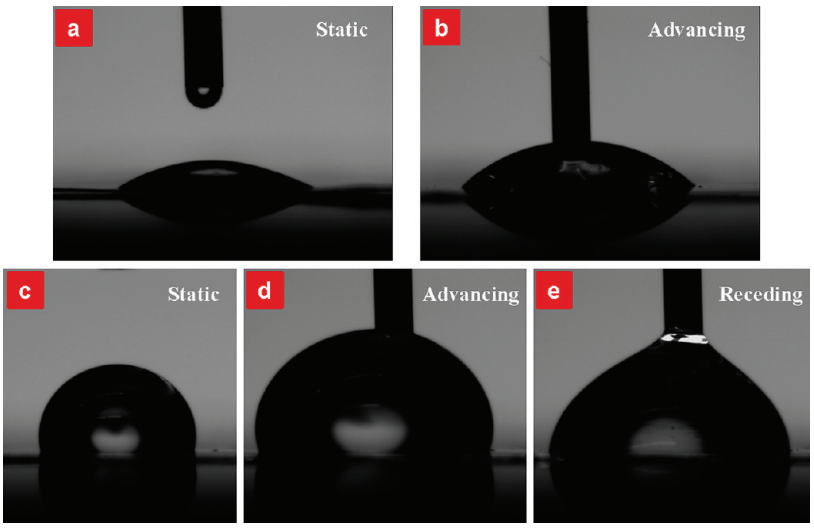

Figure 2. Telescopic images of H_2O on the AAO membrane surface before and after surface modification: (a) original AAO membrane (static); (b) original AAO membrane (advancing); (c) DMS-T22 modified AAO membrane (static); (d) DMS-T22 modified AAO membrane (advancing); (e) DMS-T22 modified AAO membrane (receding).

TABLE 1. Contact Angle of the AAO Membrane Surface before and after Surface Modification

contact angle	original AAO membrane	DMS-T22 modified AAO membrane
static	33.8°	104.7°
advancing	43.8°	109.3°
receding		92.9°

templates were synthesized according to the anodization method developed by Masuda and co-workers.[38] The resultant template contains regular and hexagonally packed pores with a center-to-center distance between the pores of ~100 nm with a pore size of ~50 nm after a pore-widening process using phosphoric acid (5 wt %) at 40 °C. Scanning force microscopy (SFM) and scanning electron microscopy (SEM) images of the AAO templates are shown in Figure 1c,d, respectively. Here, pores ~50 nm in diameter are shown, and the pore diameter could be easily controlled by the anodization conditions, for example, the electrolyte type, concentration, applied voltage, and temperature. A side view of the AAO membrane (~200 nm in length) is shown in the inset of Figure 1d. The pore length could be adjusted by varying the time of the second anodization (see Supporting Information, Figure S1).

To assess the change in the surface properties of the membrane upon coating with DMS-T22 release agent, contact angles were measured on the surface before and after the modification was performed (Figure 2, Table 1). The results show that the AAO template is much more hydrophobic after modification.

To make the nanopillar arrays of P3HT using the AAO template requires the use of the release agent. Initially, the P3HT was forced into the nanopores of the AAO template by thermal imprinting, and then the template was simply dissolved with a 5 wt % $NaOH/H_2O$ solution to release the P3HT nanoarrays. Freeze-drying was then used to remove the water under high vacuum conditions to obtain the free-standing P3HT nanoarrays. This process avoided the collapse of the nanopillars by capillary force, which would be seen if the water was simply evaporated. However, this process left a substantial amount of impurities on the surface of the nanopillars, and the $NaOH/H_2O$ was found to chemically react with the P3HT, which is not desirable for device performance. Consequently, an alternate approach, a thermal imprinting or nanoimprint lithography (NIL) process, was used where the AAO templates were modified with a DMS-T22 mold-release agent to reduce the surface energy of the templates. After thermal imprinting, the templates were easily lifted off. This NIL method gave a flat, clean array of nanorods (see Supporting Information, Figure S2).

Arrays of high areal density, free-standing P3HT nanorods (~50 nm diameter) are shown in Figure 3a–c. These nanorods afford a high interfacial area between the P3HT and electron acceptor that can be backfilled between the nanorods. No collapse of the nanostructures was observed. The microscopy images showed that the top of the pillars are not flat, but hemispherical shaped, which is exactly the same shape of the bottom side of the cylindrical pore of the AAO template; based on these, an assumption was made that the polymer was fully filled in the cylindrical pore during NIL, and the nanopillars with the aspect ratio ~4 and the spacing ~100 nm were fabricated.

The diameter of the free-standing P3HT nanorods could be easily controlled by the AAO templates; for example, smaller diameter ($D = 30$ nm) P3HT nanorods with the aspect ratio ~6.6 and the spacing ~60 nm are shown in Figure 4.

If P3HT:PCBM (1:1 wt ratio) blends were used instead of pure P3HT, free-standing P3HT:PCBM nanopillars

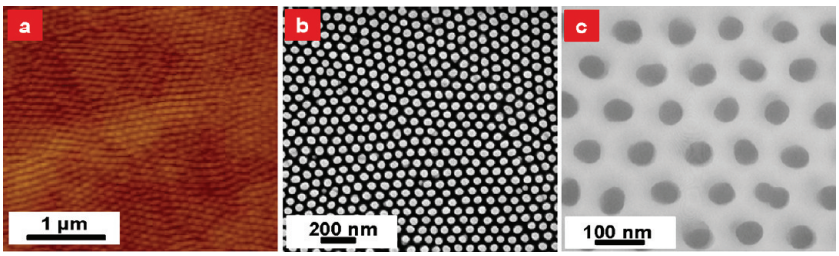

Figure 3. Micrographs of free-standing P3HT nanostructures: (a) SFM of the free-standing P3HT pillars (D = 50 nm); (b) SEM of the free-standing P3HT pillars; (c) TEM of the free-standing P3HT pillars.

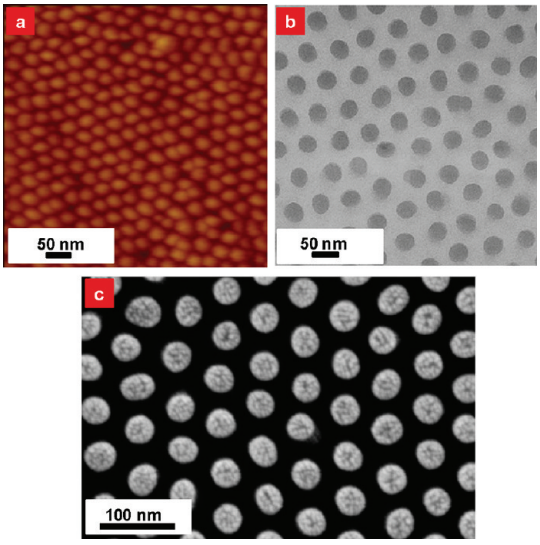

Figure 4. Micrographs of free-standing P3HT nanopillars: (a) SFM of the free-standing P3HT pillars (D = 30 nm); (b) TEM of the free-standing P3HT pillars; (c) SEM of the free-standing P3HT pillars.

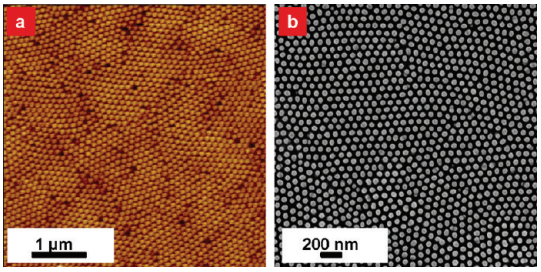

Figure 5. Micrographs of free-standing P3HT:PCBM nanopillars: (a) SFM of the free-standing P3HT:PCBM pillars (D = 50 nm); (b) SEM of the free-standing P3HT:PCBM pillars.

could also be fabricated (Figure 5). When the Al cathode was thermally evaporated onto the sample, the interface between the active layer and the cathode could be significantly increased.

Grazing incidence X-ray diffraction (GIXD) was used to determine the ordering of the components in the nanostructures. An incidence angle of 0.18°, which is above the critical angle of the P3HT (0.16°), was used to probe the ordering of the P3HT and/or PCBM throughout the sample. The diffraction data are shown in Figure 6. Figure 6a shows the 2D image for the pure P3HT arrays with nanopillars ~50 nm in diameter, while the 2D image in Figure 6b is for the P3HT: PCBM blend arrays with nanopillars ~50 nm in diameter. Both images show the (100) reflection, along with second (200) and third order (300) reflections, indicating that the edge-on crystal structure is prevalent in these samples. This means that the P3HT backbones are oriented orthogonal to the axes of the nanopillars, while the P3HT face-on structure was reported by Kim *et al.*[41] The possible reason for the different crystal orientation, as reported by Byun *et al.*[43] and Arial *et al.*,[40] is that the conformation of the hydrophobic hexyl side chains in P3HT nanorods should be adjusted to minimize the contact to the hydrophilic surface. This leads to the edge-on conformation of the P3HT chains to the hydrophilic surface. Thus, P3HT chains employed in this study should have the face-on structure on the PDMS-modified AAO surface with hydrophobic property, which results in the edge-on structure along the P3HT nanorod direction. Meanwhile, the P3HT nanorods reported by Kim *et al.* showed the face-on structure along the nanorod direction because of hydrophilic properties of the AAO wall.

In the P3HT:PCBM blend arrays, an interference arising from the PCBM (q = 1.41 Å^{-1}) is also observed. It should be noted that, with the addition of PCBM, the orientation of the P3HT is much greater and the reflection arising from the PCBM is not azimuthally uniform but, rather, shows arcs at 30° off the vertical. The 1D profile in Figure 6c is the signal from out-of-plane scattering, that is, characterizing the ordering normal to the sample surface.

Photovoltaic devices with traditional structures were prepared. Here, a PEDOT:PSS layer was cast onto ITO glass, then a ~180 nm P3HT layer was spin-coated from the P3HT chlorobenzene solution on top onto the PEDOT:PSS-coated ITO glass and the NIL process was used to generate a surface topography of the P3HT nanopillars with different diameters. A PCBM solution in dichloromethane (DCM) was spin-coated onto the P3HT thin film layer or the arrays of P3HT to form a PCBM layer. Since DCM is a marginal solvent for P3HT and can dissolve low molecular weight P3HT and swell the P3HT film or the P3HT arrays, the deposition process had to be done as rapidly as possible. Al was then evaporated onto the surface as the cathode. The device performances are summarized in Figure 7 and

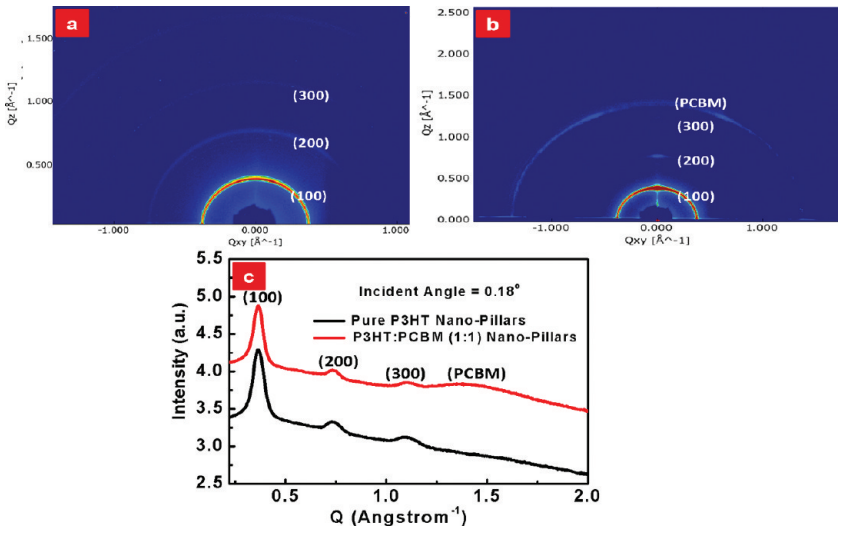

Figure 6. GIXD of the free-standing nanopillars: (a) GIXD 2D image for the pure P3HT arrays (D = ~50 nm); (b) GIXD 2D image for the P3HT:PCBM (1:1) arrays (D = ~50 nm); (c) out-of-plane 1D profile of a and b.

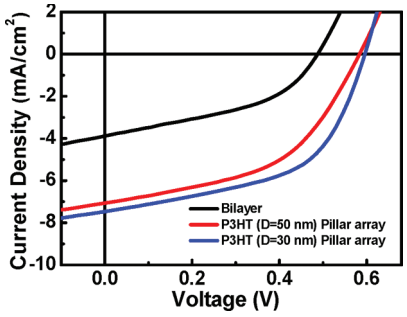

Figure 7. J–V curve of the devices based on different textures.

TABLE 2. Device Performance Based on Different Textures

device type	V_{oc} (V)	J_{sc} (mA/cm^2)	FF[a] (%)	PCE[b] (%)
bilayer	0.49	3.88	43.33	0.82
P3HT pillars (50 nm)	0.58	7.06	48.83	2.0
P3HT pillars (30 nm)	0.60	7.46	53.53	2.4

[a] Fill factor. [b] Power conversion efficiency.

Table 2. It is clear that the bilayer device shows the lowest performance, as would be expected, characterized by a relatively small open circuit voltage (V_{oc}) and short circuit current density (J_{sc}). Once the P3HT layer was converted into nanopillars with ~50 nm in diameter and then backfilled with the PCBM layer, the performance dramatically increased to ~2%, with a higher V_{oc} and J_{sc}, due to the larger surface area between the donor and acceptor domains and the vertically ordered heterojunction morphology in the active layer. When the diameters of the P3HT pillars are reduced to ~30 nm, the efficiency is even higher, due, more than likely, to reduced exciton recombination within the nanopillars since the exciton diffusion length limitation is ~10 nm. The efficiency of the P3HT/PCBM nanopillar device was 2.4%, which is comparable to that obtained by others using a standard NIL mold (quartz or Si) treated with a low surface energy release agent,[22] whereas the method presented here is simpler, much less costly, and provides easier dimensional control.

CONCLUSION

The surface energy of the AAO template was successfully reduced by DMS-T22 modification, making it suitable as an NIL template. Free-standing nanorod arrays of poly(3-hexylthiophene) (P3HT) were fabricated on ITO/glass substrates by using anodic aluminum oxide (AAO). The fabricated P3HT nanostructures dramatically increase the interfacial area between the donor and acceptor, which shortened the transporting pathway of the charge carriers and enhanced the device efficiency to around 2.4%. This technique provided new insight and guidance for the development in the photovoltaic area, as it could be easily applied to the NIL processing.

EXPERIMENTAL SECTION

Materials and Methods. Regioregular poly(3-hexylthiophene) (M_w = 42.4 k, M_n = 21.2 k, RR = 96.8%) and [6,6]-phenyl-C61-butyric acid methyl ester were obtained from Konarka Technologies. DMS-T22 was purchased from Gelest, Inc. The indium tin oxide (ITO)-coated glass substrates (20 ± 5 ohms/sq) were bought from Thin Film Devices Inc.

Preparation of Anodic Aluminum Oxide (AAO) Membranes. The AAO templates were prepared, according to published methods,[38] by the two-step anodization process developed by Masuda *et al.* At first, a high-purity aluminum sheet (99.999%, 0.25 mm thick) was polished by the grinder "PowerPro 3000". Then the sample was sonicated in water and rinsed in an acetone solution. Subsequently, the aluminum sheet was anodized at 40 V in

0.3 mol/L oxalic acid at 17 °C for 5 h. After the resultant aluminum oxide film was chemically etched in a mixture of phosphoric and chromic acid, the second anodization was performed for different time intervals ranging from 60 to 120 s, which can control the pore length in the AAO templates. Pore widening was performed using aqueous phosphoric acid (5 wt %) at 25 °C for a defined time. The nanopore center-to-center distance is ~100 nm, and the diameter is around 50 nm after the pore-widening process by using phosphoric acid. Smaller pore sizes (~30 nm) can be made by performing the anodization at 25 V in 0.3 mol/L sulfuric solution at 4 °C.

Surface Modification of the Anodic Aluminum Oxide (AAO) Membranes. AAO templates were immersed in DMS-T22 at 150 °C for 2 days, subsequently rinsed with toluene, acetone, ethanol, and DI water. Finally the substrates were dried.

Contact Angle Measurements. Contact angle measurements were performed using a tensiometer (OCA 20, Future Digital Scientific Co., Garden City, NY) and a syringe with a 24-gauge flat-tipped needle. Dynamic advancing (θ_A) and receding angles (θ_R) were recorded while Milli-Q water was added to and withdrawn from the drop, respectively.

Fabrication of P3HT Nanoarrays. A 2 wt % P3HT chlorobenzene solution was spin-coated on silicon wafers or ITO glass substrates which have been treated with O_2 plasma, at 4000 rpm for 1 min. At the same time, a 2 wt % P3HT solution in chlorobenzene was spin-coated onto the AAO templates with an underlying aluminum substrate at 1000 rpm for 1 min and dried under vacuum at room temperature. Then, both substrates coated with P3HT (one from the AAO template and the other from the silicon wafer or ITO glass substrates) were put facing each other in order to allow the P3HTs layers to interdiffuse, forming a single layer. Then, the sample was sandwiched between two glass slides and clamped together. To get better contact between the AAO template and the silicon or ITO substrate, a 5 mm thick PDMS was inserted between the AAO template and the outside glass slide. Under vacuum conditions, the sample was heated to 230 °C and annealed for 10 min at that temperature. After the sample was cooled to the room temperature, the top alumina layer was carefully removed by sand paper, and then the sample was immersed in 5 wt % $CuCl_2/H_2O$ solution for about 20 min to completely dissolve the Al layer. Subsequently, the alumina template was removed using a 5 wt % $NaOH/H_2O$ solution to release the P3HT nanoarrays. The substrate with P3HT nanoarrays was immersed in water (10 min), $EtOH/H_2O$ (1:1) (20 min), and isopropyl alcohol (IPA)/H_2O (1:1) (20 min) to remove the residue of sodium and aluminum hydroxide. Finally, the sample was transferred to a 20 mL vial filled with 1 mL of IPA/H_2O (1:1) and frozen by liquid nitrogen (N_2). The IPA and water was removed by subliming the ice under high vacuum conditions. IPA was used to make the P3HT nanorods stand normal to the surface due to their low surface energy and low volume expansion when it was frozen.

A 2 wt % P3HT solution in chlorobenzene was spin-coated on PEDOT:PSS-coated silicon wafers or ITO glass substrates at 1000 rpm for 1 min. Then the DMS-T22-modified AAO membrane with the underlying aluminum substrates were brought together with the P3HT-coated substrates, sandwiched facing each other between two glass slides and clamped together. To get better contact between AAO template and the P3HT-coated glass or ITO substrate, a 5 mm thick PDMS was inserted between the AAO template and the outside glass slide. The sample was heated to 230 °C under vacuum and annealed for 5 min at that temperature. After the sample cooled to room temperature, the templates were easily demolded, leaving the nanostructure behind on the P3TH thin film.

Organic Solar Cell Devices Fabrication and Testing. ITO-coated glass substrates were cleaned through ultrasonication treatment in detergent, DI water, acetone, and isopropyl alcohol and then dried in an oven overnight. PEDOT:PSS (CLEVIOS P VP AI 4083) (~35 nm) was spin-coated onto ultraviolet ozone-treated ITO substrates. After annealing at 150 °C for 30 min in air, the substrates were transferred to a glovebox. P3HT thin films were spin-coated onto the substrates where the thickness of the P3HT film was ~180 nm (KLA-TENCOR Alpha-Step IQ Surface Profiler). Nanostructured P3HT surfaces were prepared by the NIL method described above. The PCBM layer was spin-coated directly on top of the P3HT nanostructured layer from a dichloromethane solution (10 mg/mL) at 3000 rpm to backfill the nanopillar array and formed a continuous PCBM thin film on top. This process was conducted as rapidly as possible to minimize interfacial mixing. Afterward, a thin (~100 nm) layer of aluminum was thermally evaporated under high vacuum (2×10^{-4} Pa) onto the surface (area 6 mm^2) as the cathode. The preparation procedure is shown in the Scheme 1. All current density−voltage ($J-V$) characteristics of the devices were measured under simulated AM1.5G irradiation (100 mW cm^{-2}) using a Xe lamp-based Newport 91160 300 W solar simulator as the white light source. The light intensity was adjusted with an NREL-calibrated Si solar cell with a KG-5 filter.

Scanning Electron Microscopy (SEM). The FEI Magellan 400 field emission scanning electron microscope was used to investigate the polymer nanostructures. All samples were coated with 3 nm Au before performing SEM measurements.

Transmission Electron Microscopy (TEM). Bright-field transmission electron microscopy (TEM) studies were conducted with a JEOL 2000 FX TEM operating at an accelerating voltage of 200 kV.

Grazing Incidence X-ray Diffraction (GIXD). GIXD measurements were performed on Beamline 7.3.3 at the Advanced Light Source at the Lawrence Berkeley National Laboratory. The experimental setup and sample cell were designed for surface studies on thin films. An X-ray beam impinged onto the sample at a grazing angle above the critical angle of the polymer film ($\alpha_c = 0.16$) but below the critical angle of the silicon substrate ($\alpha_c = 0.22$). The wavelength of X-rays used was 1.240 Å, and the scattered intensity was detected using a two-dimensional charge-coupled device (CCD) camera with image sizes of 2304 × 2304 pixels, pixel size is 0.082 mm × 0.082 mm.

Acknowledgment. We thank Prof. Jean M.J. Fréchet for his suggestion at the beginning of this project. This work was supported by the Department of Energy through the Energy Frontier Research Center at the University of Massachusetts (DOE DE-PS02-08ER15944), the NSF-supported Materials Research Science and Engineering Center at the University of Massachusetts (DMR-0820506), portions of this research were carried out at the Advanced Light Source, Berkeley National Laboratory, which was supported by the DOE, Office of Science, and Office of Basic Energy Sciences.

Supporting Information Available: Nanopore length growth rate in the AAO template; optical micrographs of arrays of P3HT nanoposts prepared by dissolution of AAO membranes and by NIL. This material is available free of charge *via* the Internet at http://pubs.acs.org.

REFERENCES AND NOTES

1. Brabec, C. J.; Sariciftci, N. S.; Hummelen, J. C. Plastic Solar Cells. *Adv. Funct. Mater.* **2001**, *11*, 15–26.
2. Yu, G.; Gao, J.; Hummelen, J. C.; Wudl, F.; Heeger, A. J. Polymer Photovoltaic Cells—Enhanced Efficiencies *via* a Network of Internal Donor−Acceptor Heterojunctions. *Science* **1995**, *270*, 1789–1791.
3. Halls, J. J. M.; Pichler, K.; Friend, R. H.; Moratti, S. C.; Holmes, A. B. Exciton Diffusion and Dissociation in a Poly(*p*-phenylenevinylene)/C-60 Heterojunction Photovoltaic Cell. *Appl. Phys. Lett.* **1996**, *68*, 3120–3122.
4. Markov, D. E.; Amsterdam, E.; Blom, P. W. M.; Sieval, A. B.; Hummelen, J. C. Accurate Measurement of the Exciton Diffusion Length in a Conjugated Polymer Using a Heterostructure with a Side-Chain Cross-Linked Fullerene Layer. *J. Phys. Chem. A* **2005**, *109*, 5266–5274.
5. Markov, D. E.; Tanase, C.; Blom, P. W. M.; Wildeman, J. Simultaneous Enhancement of Charge Transport and Exciton Diffusion in Poly(*p*-phenylene vinylene) Derivatives. *Phys. Rev. B* **2005**, *72*, 045217.
6. Hoppe, H.; Sariciftci, N. S. Morphology of Polymer/Fullerene Bulk Heterojunction Solar Cells. *J. Mater. Chem.* **2006**, *16*, 45–61.

7. Ma, W. L.; Yang, C. Y.; Gong, X.; Lee, K.; Heeger, A. J. Thermally Stable, Efficient Polymer Solar Cells with Nanoscale Control of the Interpenetrating Network Morphology. *Adv. Funct. Mater.* **2005**, *15*, 1617–1622.
8. Chen, D. A.; Nakahara, A.; Wei, D. G.; Nordlund, D.; Russell, T. P. P3HT/PCBM Bulk Heterojunction Organic Photovoltaics: Correlating Efficiency and Morphology. *Nano Lett.* **2011**, *11*, 561–567.
9. Chen, D.; Liu, F.; Wang, C.; Nakahara, A.; Russell, T. P. Bulk Heterojunction Photovoltaic Active Layers *via* Bilayer Interdiffusion. *Nano Lett.* **2011**, *11*, 2071–2078.
10. Zhao, Y.; Xie, Z. Y.; Qu, Y.; Geng, Y. H.; Wang, L. X. Solvent-Vapor Treatment Induced Performance Enhancement of Poly(3-hexylthiophene): Methanofullerene Bulk-Heterojunction Photovoltaic Cells. *Appl. Phys. Lett.* **2007**, *90*, 043504.
11. Jo, J.; Na, S. I.; Kim, S. S.; Lee, T. W.; Chung, Y.; Kang, S. J.; Vak, D.; Kim, D. Y. Three-Dimensional Bulk Heterojunction Morphology for Achieving High Internal Quantum Efficiency in Polymer Solar Cells. *Adv. Funct. Mater.* **2009**, *19*, 2398–2406.
12. van Bavel, S. S.; Sourty, E.; de With, G.; Loos, J. Three-Dimensional Nanoscale Organization of Bulk Heterojunction Polymer Solar Cells. *Nano Lett.* **2009**, *9*, 507–513.
13. Park, S. H.; Roy, A.; Beaupre, S.; Cho, S.; Coates, N.; Moon, J. S.; Moses, D.; Leclerc, M.; Lee, K.; Heeger, A. J. Bulk Heterojunction Solar Cells with Internal Quantum Efficiency Approaching 100%. *Nat. Photonics* **2009**, *3*, 297–302.
14. Mayer, A. C.; Toney, M. F.; Scully, S. R.; Rivnay, J.; Brabec, C. J.; Scharber, M.; Koppe, M.; Heeney, M.; McCulloch, I.; McGehee, M. D. Bimolecular Crystals of Fullerenes in Conjugated Polymers and the Implications of Molecular Mixing for Solar Cells. *Adv. Funct. Mater.* **2009**, *19*, 1173–1179.
15. Peet, J.; Kim, J. Y.; Coates, N. E.; Ma, W. L.; Moses, D.; Heeger, A. J.; Bazan, G. C. Efficiency Enhancement in Low-Bandgap Polymer Solar Cells by Processing with Alkane Dithiols. *Nat. Mater.* **2007**, *6*, 497–500.
16. Chen, H. Y.; Yang, H. C.; Yang, G. W.; Sista, S.; Zadoyan, R. B.; Li, G.; Yang, Y. Fast-Grown Interpenetrating Network in Poly(3-hexylthiophene): Methanofullerenes Solar Cells Processed with Additive. *J. Phys. Chem. C* **2009**, *113*, 7946–7953.
17. Moule, A. J.; Meerholz, K. Controlling Morphology in Polymer−Fullerene Mixtures. *Adv. Mater.* **2008**, *20*, 240–245.
18. Lee, J. K.; Ma, W. L.; Brabec, C. J.; Yuen, J.; Moon, J. S.; Kim, J. Y.; Lee, K.; Bazan, G. C.; Heeger, A. J. Processing Additives for Improved Efficiency from Bulk Heterojunction Solar Cells. *J. Am. Chem. Soc.* **2008**, *130*, 3619–3623.
19. Rogers, J. T.; Schmidt, K.; Toney, M. F.; Kramer, E. J.; Bazan, G. C. Structural Order in Bulk Heterojunction Films Prepared with Solvent Additives. *Adv. Mater.* **2011**, *23*, 2284–2288.
20. Tai, Q. D.; Zhao, X. Z.; Yan, F. Hybrid Solar Cells Based on Poly(3-hexylthiophene) and Electrospun TiO_2 Nanofibers with Effective Interface Modification. *J. Mater. Chem.* **2010**, *20*, 7366–7371.
21. Haberkorn, N.; Gutmann, J. S.; Theato, P. Template-Assisted Fabrication of Free-Standing Nanorod Arrays of a Hole-Conducting Cross-Linked Triphenylamine Derivative: Toward Ordered Bulk-Heterojunction Solar Cells. *ACS Nano* **2009**, *3*, 1415–1422.
22. Aryal, M.; Buyukserin, F.; Mielczarek, K.; Zhao, X. M.; Gao, J. M.; Zakhidov, A.; Hu, W. C. Imprinted Large-Scale High Density Polymer Nanopillars for Organic Solar Cells. *J. Vac. Sci. Technol., B* **2008**, *26*, 2562–2566.
23. Wang, H. S.; Lin, L. H.; Chen, S. Y.; Wang, Y. L.; Wei, K. H. Ordered Polythiophene/Fullerene Composite Core−Shell Nanorod Arrays for Solar Cell Applications. *Nanotechnology* **2009**, *20*, 075201.
24. He, X. M.; Gao, F.; Tu, G. L.; Hasko, D.; Huttner, S.; Steiner, U.; Greenham, N. C.; Friend, R. H.; Huck, W. T. S. Formation of Nanopatterned Polymer Blends in Photovoltaic Devices. *Nano Lett.* **2010**, *10*, 1302–1307.
25. He, X. M.; Gao, F.; Tu, G. L.; Hasko, D. G.; Huttner, S.; Greenham, N. C.; Steiner, U.; Friend, R. H.; Huck, W. T. S. Formation of Well-Ordered Heterojunctions in Polymer: PCBM Photovoltaic Devices. *Adv. Funct. Mater.* **2011**, *21*, 139–146.
26. Coakley, K. M.; McGehee, M. D. Conjugated Polymer Photovoltaic Cells. *Chem. Mater.* **2004**, *16*, 4533–4542.
27. Mayer, A. C.; Scully, S. R.; Hardin, B. E.; Rowell, M. W.; McGehee, M. D. Polymer-Based Solar Cells. *Mater. Today* **2007**, *10*, 28–33.
28. Gunes, S.; Neugebauer, H.; Sariciftci, N. S. Conjugated Polymer-Based Organic Solar Cells. *Chem. Rev.* **2007**, *107*, 1324–1338.
29. Steinhart, M.; Wendorff, J. H.; Greiner, A.; Wehrspohn, R. B.; Nielsch, K.; Schilling, J.; Choi, J.; Gosele, U. Polymer Nanotubes by Wetting of Ordered Porous Templates. *Science* **2002**, *296*, 1997–1997.
30. Steinhart, M.; Wehrspohn, R. B.; Gosele, U.; Wendorff, J. H. Nanotubes by Template Wetting: A Modular Assembly System. *Angew. Chem., Int. Ed.* **2004**, *43*, 1334–1344.
31. Moon, S. I.; McCarthy, T. J. Template Synthesis and Self-Assembly of Nanoscopic Polymer "Pencils". *Macromolecules* **2003**, *36*, 4253–4255.
32. Zhang, M. F.; Dobriyal, P.; Chen, J. T.; Russell, T. P.; Olmo, J.; Merry, A. Wetting Transition in Cylindrical Alumina Nanopores with Polymer Melts. *Nano Lett.* **2006**, *6*, 1075–1079.
33. Feng, X. D.; Jin, Z. X. Spontaneous Formation of Nanoscale Polymer Spheres, Capsules, or Rods by Evaporation of Polymer Solutions in Cylindrical Alumina Nanopores. *Macromolecules* **2009**, *42*, 569–572.
34. Chen, J. T.; Chen, D.; Russell, T. P. Fabrication of Hierarchical Structures by Wetting Porous Templates with Polymer Microspheres. *Langmuir* **2009**, *25*, 4331–4335.
35. Chen, D.; Park, S.; Chen, J. T.; Redston, E.; Russell, T. P. A Simple Route for the Preparation of Mesoporous Nanostructures Using Block Copolymers. *ACS Nano* **2009**, *3*, 2827–2833.
36. Wang, Y.; Gosele, U.; Steinhart, M. Mesoporous Block Copolymer Nanorods by Swelling-Induced Morphology Reconstruction. *Nano Lett.* **2008**, *8*, 3548–3553.
37. Zhao, W.; Chen, D.; Hu, Y. X.; Grason, G. M.; Russell, T. P. ABC Triblock Copolymer Vesicles with Mesh-like Morphology. *ACS Nano* **2011**, *5*, 486–492.
38. Masuda, H.; Fukuda, K. Ordered Metal Nanohole Arrays Made by a 2-Step Replication of Honeycomb Structures of Anodic Alumina. *Science* **1995**, *268*, 1466–1468.
39. Chen, J. T.; Shin, K.; Leiston-Belanger, J. M.; Zhang, M. F.; Russell, T. P. Amorphous Carbon Nanotubes with Tunable Properties *via* Template Wetting. *Adv. Funct. Mater.* **2006**, *16*, 1476–1480.
40. Aryal, M.; Trivedi, K.; Hu, W. C. Nano-Confinement Induced Chain Alignment in Ordered P3HT Nanostructures Defined by Nanoimprint Lithography. *ACS Nano* **2009**, *3*, 3085–3090.
41. Kim, J. S.; Park, Y.; Lee, D. Y.; Lee, J. H.; Park, J. H.; Kim, J. K.; Cho, K. Poly(3-hexylthiophene) Nanorods with Aligned Chain Orientation for Organic Photovoltaics. *Adv. Funct. Mater.* **2010**, *20*, 540–545.
42. Krumpfer, J. W.; McCarthy, T. J. Rediscovering Silicones: "Unreactive" Silicones React with Inorganic Surfaces. *Langmuir* **2011**, *27*, 11514–11519.
43. Byun, J.; Kim, Y.; Jeon, G.; Kim, J. K. Ultrahigh Density Array of Free-Standing Poly(3-hexylthiophene) Nanotubes on Conducting Substrates *via* Solution Wetting. *Macromolecules* **2011**, *44*, 8558–8562.